NANO LETTERS

pubs.acs.org/NanoLett Letter

Toward Controlled Synthesis of 2D Crystals by CVD: Learning from the Real-Time Crystal Morphology Evolutions

Jing Zhang,[§] Tianshu Zhai,[§] Faizal Arifurrahman, Yuguo Wang, Andrew Hitt, Zelai He, Qing Ai, Yifeng Liu, Chen-Yang Lin, Yifan Zhu, Ming Tang,* and Jun Lou*

Cite This: *Nano Lett.* 2024, 24, 2465−2472 Read Online

ACCESS | Metrics & More | Article Recommendations | Supporting Information

ABSTRACT: The rich morphology of 2D materials grown through chemical vapor deposition (CVD), is a distinctive feature. However, understanding the complex growth of 2D crystals under practical CVD conditions remains a challenge due to various intertwined factors. Real-time monitoring is crucial to providing essential data and enabling the use of advanced tools like machine learning for unraveling these complexities. In this study, we present a custom-built miniaturized CVD system capable of observing and recording 2D MoS_2 crystal growth in real time. Image processing converts the real-time footage into digital data, and machine learning algorithms (ML) unveil the significant factors influencing growth. The machine learning model successfully predicts CVD growth parameters for synthesizing ultralarge monolayer MoS_2 crystals. It also demonstrates the potential to reverse engineer CVD growth parameters by analyzing the as-grown 2D crystal morphology. This interdisciplinary approach can be integrated to enhance our understanding of controlled 2D crystal synthesis through CVD.

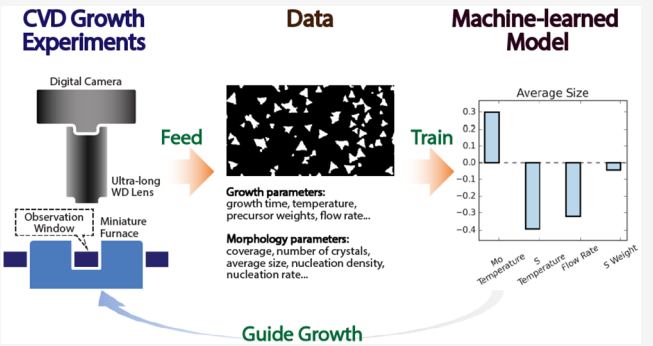

KEYWORDS: *MoS_2 morphology, miniaturized CVD, image processing, machine-learning, growth model and prediction*

The development of the CVD technique to grow large single-crystalline van der Waals (VdW) monolayer materials has been very successful in the past decade. A wide variety of 2D monolayers and few layers including graphene,[1] hBN,[2] MoS_2 and its family,[3,4] SnS_2,[5] GaSe,[6] perovskite, and more have been grown successfully using CVD.[7] Despite the substantial growth of the number of publications on CVD growth of 2D materials, there still exist inconsistencies of the correlations between the growth conditions and the crystal morphologies from different reports. For example, Wang et. al reported the shape evolution of CVD-grown MoS_2 from triangles to hexagons as the MoO_3/S ratio drops,[8] while Yang et. al reported otherwise.[9] Those disagreements are oftentimes confusing and cannot be neglected if we aim to push this technique toward industry applications. A clearer picture of the 2D crystal growth must be developed to better understand the underlying growth mechanism before consistent and reproducible CVD growth can be demonstrated. Additionally, there is abundant evidence suggesting the hidden link between the crystal morphologies and their chemical/physical properties.[10−15] Therefore, by controlling the growth condition of 2D crystals and their correlated morphologies, it is possible to rationally engineer these materials with desired properties.[16]

It is well recognized that direct observation of crystal morphology evolution plays an irreplaceable role in understanding the growth mechanism of materials.[17,18] Dynamic morphology evolution of crystals at different periods of growth, when correlated with real-time growth conditions, can not only correct misinterpreted growth process−experimental parameter correlations (e.g., false assumption that the growth ends at a specific point on the ramping-cooling curve) but also deliver important information (e.g., sequence of nucleation events and competition of growth of crystals with different sizes) that are usually missing in conventional growth experiments with only snapshots of starting and ending points of the growth processes. For example, recent progress has shown direct observations of 2D PbI_2 growth on MoS_2.[19] The latest development has also demonstrated that a more challenging experiment of direct observation of graphene single crystal growth on top of liquid metal substrate can be done with a customized reaction chamber.[20,21] It is worth noting that transition-metal dichalcogenides (TMDs) such as MoS_2 are one of the most important 2D materials beyond graphene, and

Received: October 19, 2023
Revised: February 2, 2024
Accepted: February 5, 2024
Published: February 13, 2024

https://doi.org/10.1021/acs.nanolett.3c04016
Nano Lett. 2024, 24, 2465−2472

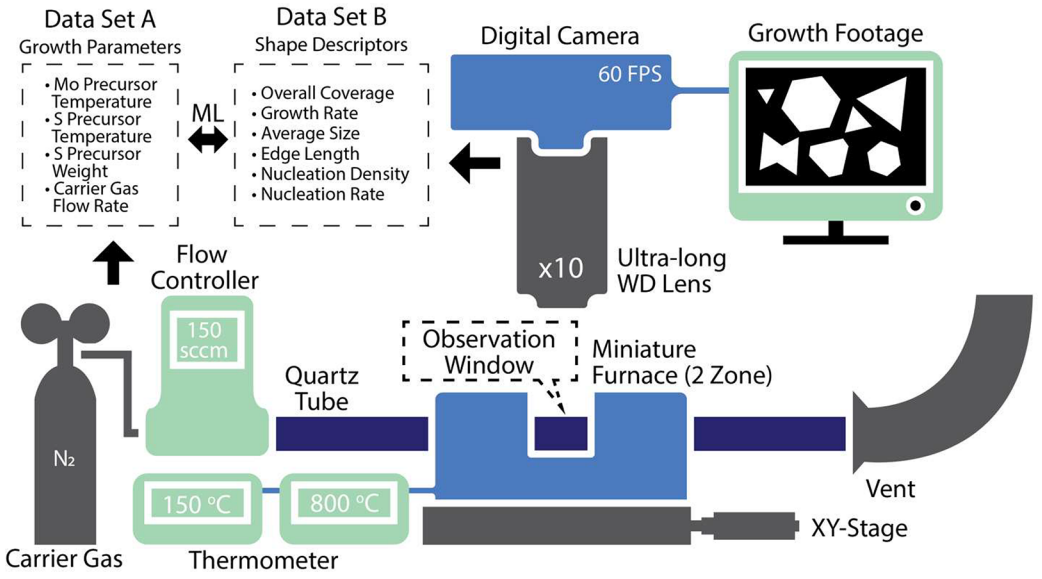

Figure 1. Schematic illustration of the workflow established in this work. The bottom half of the panel represents the growth footage capturing sector. The top right of the panel represents the growth footage digitizing sector. The top left of the panel represents the machine-learning sector. The reaction parameters shown are examples representing one specific growth condition.

MoS_2 has its own growth mechanism that is completely different from graphene.[22] Until now there was only a limited number of reports on the direct observation of TMD growth in CVD using high-end TEM reaction chambers[23] and optical microscope-based setups.[24,25] While the very early stage of crystal nucleation could be observed in TEM at a very high magnification, which inherently has a very small observation window, this type of technique uses a different reaction chamber layout compared to commonly used tube-furnace based CVD syntheses. As a result, lots of the phenomena that matter in a conventional TMD growth, especially those related to fundamental growth mechanisms, such as the competition between nucleation and growth of different crystals throughout the growth period and Oswald ripening of neighboring crystals,[26] and those related to final product morphology control, such as overall coverage,[27] orientation of different crystals and grain boundary density,[28,29] are very challenging to be directly observed from the TEM-based growth experiment. For earlier optical microscope-based setups, due to the limitation imposed by the optics on top of the growth chamber, the orientation of growth substrate and position of the precursors are compromised and do not represent the conventional CVD layout. Therefore, it is imperative to develop another approach that could better mimic the conventional CVD growth conditions while offering direct observation capabilities to better understand the underlying growth mechanism of 2D TMD crystals.

On the other hand, as multiple crystals form, merge, and grow on the same substrate, it is important to track the morphology information on each crystal so that a comprehensive picture on the growth mechanism can be drawn. To do that, the obtained material growth footage must first be digitized, and then the morphology parameters such as crystal lateral size and growth rate need to be quantified. With such information, powerful tools such as ML algorithms can be employed to process the shear amount of data and help building models to predict and control 2D crystal growth. It is also worth noting that the fast development in implementing machine-learning (ML) techniques into practical engineering processes in recent years has promoted the application of ML approach in 2D TMDs-related studies, including data-mining based assessment of CVD growth process,[30] Raman spectra identification,[31] defect dynamics, and growth condition control.[32,33] So time is ripe to integrate an advanced growth system with the capability of observing and recording the growth of 2D TMD crystals in real time with powerful ML algorithms to better understand their underlying growth mechanisms toward controlled scalable synthesis. Beyond that, real-time CVD plus ML will not only allow us to validate many 2D material growth theories based on ab initio and first-principle calculations but also provide much larger and richer data set than traditional CVD growth process as the ground truth to improve the machine-learning models.

In this work, we have established a complete workflow for such purposes and demonstrated its capability in guiding the CVD growth of MoS_2 monolayers (Figure 1). The workflow consists of utilizing a custom-built miniaturized CVD apparatus integrated with an optical microscope to capture the 2D MoS_2 crystal growth footage, applying computer-based image processing algorithms to digitize the growth footage, and then using machine-learning-enabled analysis to understand the correlation between the obtained crystal morphology parameters and the growth experiment conditions. More importantly, we have demonstrated important applications of such a workflow in guiding controlled growth to achieve desired crystal morphologies as well as figuring out the growth conditions by analyzing the obtained crystal morphology parameters.

In our workflow, the first step is to record the whole growth process with a digital camera. There are several practical challenges when simply trying to reduce the size of a conventional CVD setup and mount a digital camera above a CVD furnace. First, there must be an open region on the furnace to allow an unblocked optical view on the sample. Second, Si with an oxidation layer can no longer be used as the growth substrate, because in order to observe the growth from above the furnace, the substrate must be transparent (as the high quality 2D crystal growth typically occurs on the bottom

https://doi.org/10.1021/acs.nanolett.3c04016
Nano Lett. 2024, 24, 2465−2472

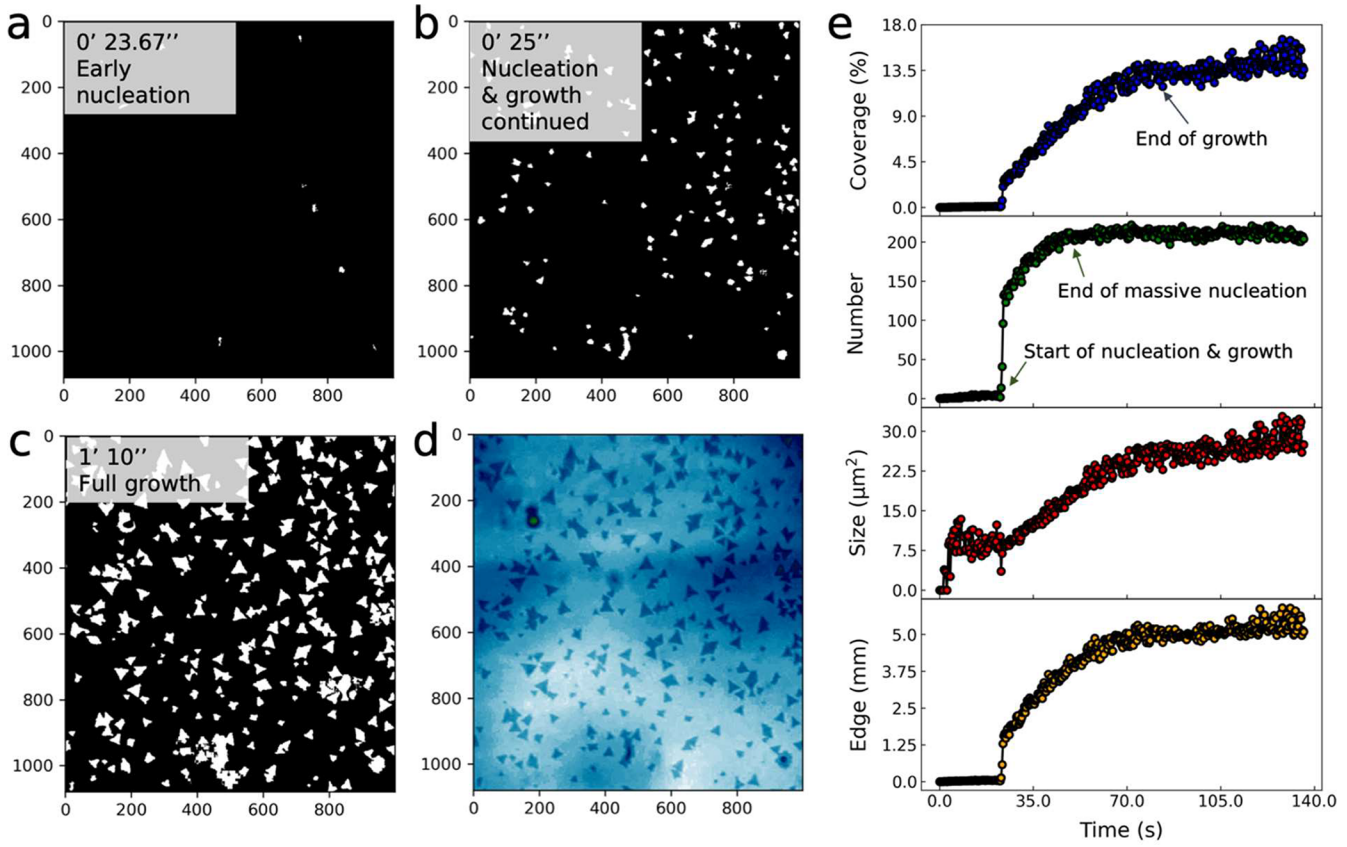

Figure 2. Digitizing the growth footage to extract time-dependent information on crystal nucleation and growth. (a) − (c) Binarized snapshots of the sample at different times. (d) False-color image of (c) before processing, in which MoS_2 flakes appear as triangular domains. Units for images (a)-(d) are all pixels. (e) Time dependence of the overall area coverage, crystal number, average crystal size, and total edge length of all crystals evaluated from the growth footage of the MoS_2 sample.

side of the growth substrates). Third, the objective lens needs to have an ultralong working distance so there would be enough space between the lens and the furnace heating zone to allow appropriate air cooling of the objective lens. We designed a custom-built miniaturized CVD system to address those challenges. The system is made of a miniaturized CVD furnace with an observation window, a rectangular quartz tubing, and an optical microscope with ultralong working distance objective lens (Figure S1). The commonly used layout of Mo, S precursors, and substrate in a conventional CVD system is retained in our system, except that Si is replaced by sapphire to allow optical transparency of the growth substrate. With this setup, what can be achieved in a conventional CVD can be preserved to the largest extent, while real-time observation and recording of the growth process become possible.

A typical growth experiment performed in such a miniaturized CVD setup produces triangular crystals on the sapphire substrate (Figure S5a). Two Raman peaks at 385.6 and 404.4 cm^{-1} can be identified exclusively from the as-grown crystals (Figure S2). These peak positions correspond to the E^1_{2g} and A_{1g} vibration modes of MoS_2, and the peak-to-peak distance of 18.8 cm^{-1} further suggests that they are monolayer MoS_2 crystals.[34,35] A strong peak in photoluminescence (PL) spectra around 1.88 eV and PL mapping (Figure S5) of the crystal confirms the findings from the Raman spectra analysis (Figure S3).[36] The AFM image (the height profile) also shows the crystal thickness of 0.6 nm matching the thickness of a monolayer MoS_2 (Figure S4).[34,37] Based on these characterization results, we confirmed that we have successfully grown MoS_2 monolayers on the sapphire substrate using the miniaturized CVD setup.

A typical footage of monolayer MoS_2 growth using the miniaturized CVD is shown as an example to demonstrate the capability of the system (Supplementary video 1). 2D MoS_2 crystals are emerging as dynamically expanding triangular domains with darker contrast, which is visually different from the commonly seen purplish flakes on the SiO_2/Si substrate. In the footage, a complete CVD growth process of MoS_2 crystals was recorded, where the crystal nucleation, growth, and coalescence and the termination of such growth can all be visually identified. A lot of useful information that was missed in conventional observations of the CVD growth is therefore revealed. For instance, this particular footage directly shows that there is a sequence among different MoS_2 crystals to nucleate, suggesting the potential importance of nucleation competition (if there is any) among neighboring crystals during the early growth stage. The footage also reveals that the majority of crystal growth happens in the time scale from tens of seconds to several minutes.

The goal of the next step is to convert the CVD growth footage (growth videos) into quantitative metrics of interest to researchers and suitable for further computer analysis. In order to do that, the contrast of MoS_2 crystals in the videos needs to be first enhanced so they can be identified by appropriately setting threshold of pixel brightness values. As mentioned earlier, transparent substrates such as sapphire do not show high contrast images naturally like SiO_2/Si substrates do (Figure 2d). However, image processing algorithms can be

https://doi.org/10.1021/acs.nanolett.3c04016
Nano Lett. 2024, 24, 2465−2472

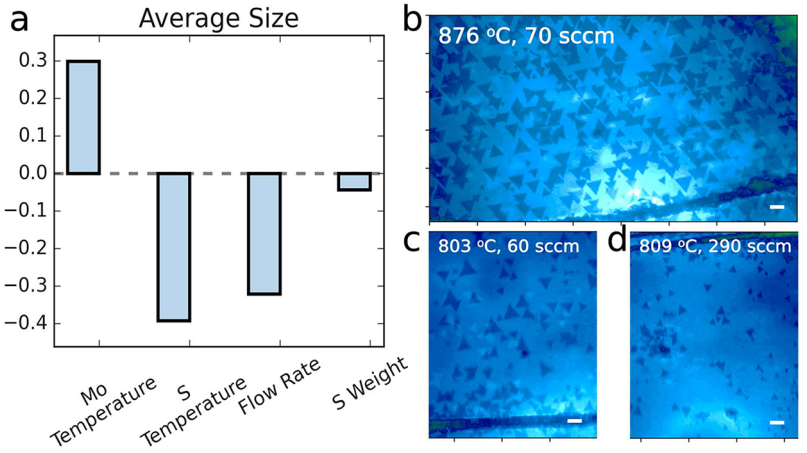

Figure 3. Machine-learning model prediction of average crystal size of miniaturized-CVD-grown MoS_2 monolayers. (a) Machine-learned feature ranking of growth controlling factors. The *y*-axis indicates the significance of these parameters in determining the average size of MoS_2 (b) False-color optical image of the MoS_2 crystals grown at a high temperature and low flow rate, where the largest average crystal size is obtained among the tested growth conditions. Scale bar: 20 μm (c) Reducing growth temperature decreases the crystal size. Scale bar: 20 μm (d) Increasing flow rate significantly reduces the crystal size. Scale bar: 20 μm.

applied to enhance the contrast in the footage. By converting the image from color mode into grayscale, the MoS_2 flakes start to show improved contrast (Figure S6b). Further contrast enhancement can be achieved by applying adaptive histogram equalization to the image (Figure S6c). Artifacts from the objective lens such as dirt can be removed by using a blank substrate image as a background and subtracting it from every frame of the video. After this step a higher quality image with a more uniform background is obtained and ready for binarization by selecting an appropriate brightness threshold (Figure S6d,e). In the binarized image, isolated crystals can be identified using a contour-finding algorithm. Lastly, noise such as small sized speckles in the binary image can be removed by applying a size filter to all identified crystals (Figure S6f). Images processed by this workflow highlight the shape features of the grown crystals and are suitable for further analysis to extract key information on crystal morphology such as shape, size, and orientation can be extracted.

The established image processing workflow is applied to every frame in the video footage. The process of the nucleation of multiple crystals and their growth from small dots into fully developed triangles can be clearly seen from the snapshots at different times (Figure 2a−c, Figure S7, and Figure S8a−c). As previously mentioned, image processing packages, such as OpenCV can be used to identify the features of each individual crystal and crystal cluster. In the current workflow, we track the number of crystals, the cumulative crystal areal coverage, and the overall edge length of the crystals as a function of the real growth time (Figure 2e). Crystal growth kinetics could be inferred from the time dependence of these morphology parameters. Other features of individual crystals, such as their size, shape, and orientation distributions and spatial correlation, will be extracted in an updated workflow to provide additional insights on the growth mechanisms of the 2D crystals. The specific growth footage shown in Figure 2e reveals several notable features of the CVD process. First, burst nucleation of MoS_2 crystals occurred after an incubation period. The majority (>50%) of the crystal nuclei emerged in the field of view in a very short time period (within several seconds). The remaining crystals formed in the subsequent 15 s, after which the nucleation rate dropped to zero. Second, the growth of crystals exhibits a similar two-stage process. After the burst nucleation, the crystal average size and areal coverage steadily increased before stagnating at ∼70 s (Figure 2e). The reduction in the nucleation and growth rates reflects the gradual decrease of the precursor supersaturation above the substrate during the CVD process due to the exhaustion of the Mo and/or S precursors. In another example (Figure S8b,c), the number of crystal islands declined after reaching a maximum at ∼27 s (Figure S8d) because of the coalescence of individual crystals. The quantification of the time dependence of the crystal nucleation, growth and morphology from the in situ observation offers valuable insights on the control of the CVD process. For example, it shows that it is important to suppress the burst nucleation event to enhance the 2D crystal size.

A couple of previous studies have compared the MoS_2 crystal morphologies at different growth temperatures and precursor layouts, showing convincing evidence that these parameters have a critical effect on the crystal morphology determination.[8,9,22] However, none of the studies includes more than two growth parameters at the same time in their comparison due to the challenge in the manual analysis of multiple controlling factors. Feature selection in machine learning provides an excellent tool to tackle such problems.[38] We choose MoO_3 growth temperature, S temperature and weight, and flow rate as the input features (X). In the experiments, their respective values were independently varied, which is evidenced by their correlation matrix (Figure S9) being close to a unit matrix. Crystal morphology descriptors including coverage, average size, edge length density, nucleation density, nucleation rate, growth rate, and grain boundary density are listed as output features (Y). A multiple linear regression model can be built based on these data sets. Methods to select the most relevant input features for each morphology descriptor, which include recursive feature addition (RFA) and elimination (RFE), and exhaustive search for the optimal combination are used to determine the feature sets (Figure S11). In an example of the selected feature set determined by the exhaustive combination search (Figure S12), the correlations of relevant growth parameters (selected features) on each morphology parameter are shown as bar

https://doi.org/10.1021/acs.nanolett.3c04016
Nano Lett. 2024, 24, 2465−2472

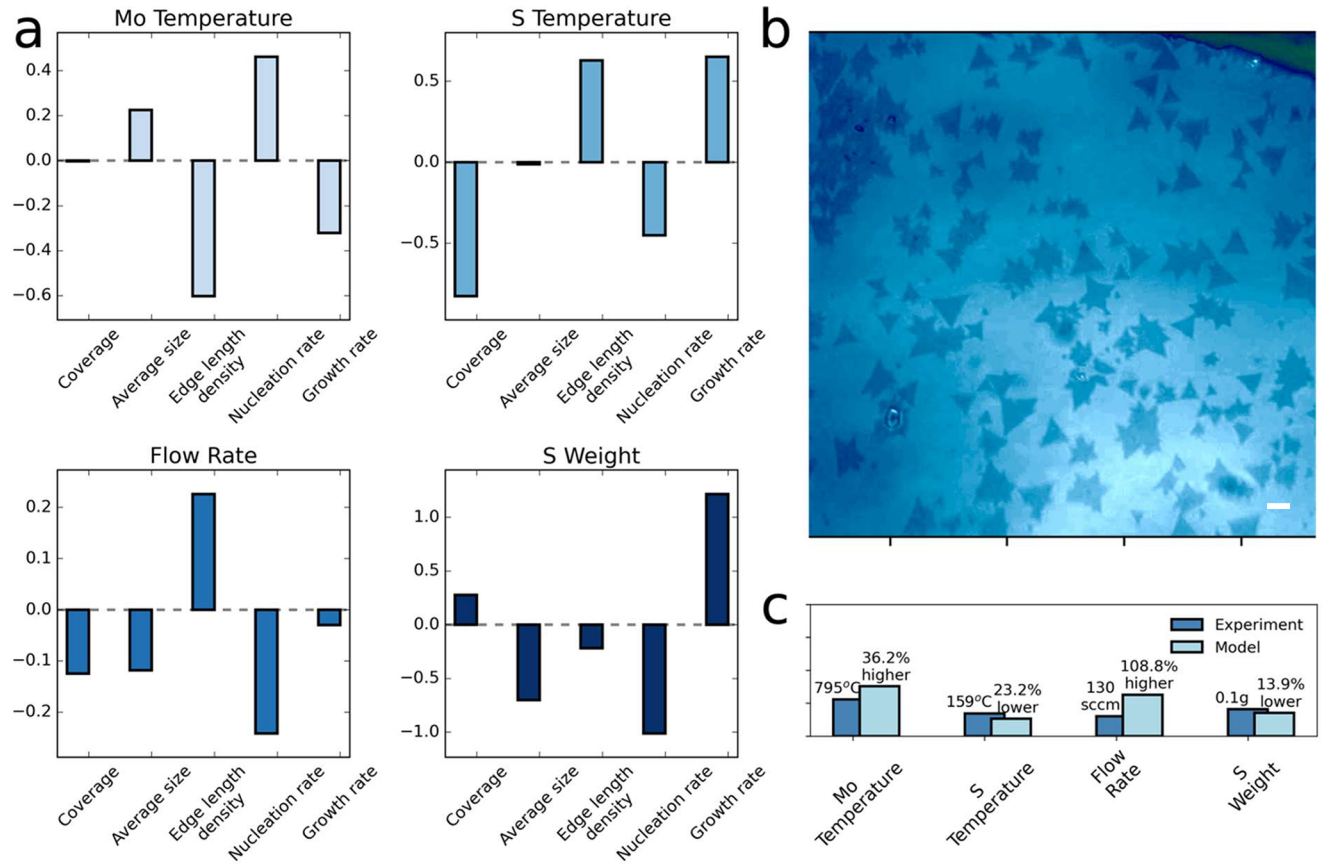

Figure 4. "A letter from the glow" − decipher growth condition from growth footage. (a) Machine-learning model showing the correlation between the four growth parameters and five morphology parameters. The *y*-axis indicates the correlation strength of these morphology parameters to the growth parameters. (b) False-color snapshot of a completely grown MoS_2 monolayer sample. Scale bar: 20 μm (c) Comparison of growth parameters predicted by the machine-learning model and their actual experimental values. The percentage difference between the model and the experiment, using the experiment as the baseline, is labeled in the figure.

plots. Comparison of all plots reveals that the MoO_3 temperature has a high ranking of importance (strong correlation) for the highest number (six out of seven) of morphology descriptors.

An important application of the feature analysis is to control and guide the material growth process based on the machine-learning prediction. Taking the average MoS_2 crystal size for example, we plot the coefficients (*y*-axis) of linear regression of each input features (X) including MoO_3 temperature, S temperature and weight, and flow rate (*x*-axes) in Figure 3a. The *y*-axis indicates the significance of these parameters in determining the final average size of MoS_2; the scale and symbol of the values represent how strong the dependencies are and whether the correlation is positive or negative. When large-sized crystals are desired, the model predicts that higher MoO_3 temperature, lower S temperature, and lower flow rate would push the growth toward the right direction. In fact, experimental observation that increasing MoO_3 temperature leads to enlarged crystal size has been reported in a previous study,[22] in agreement with our machine-learning model prediction. The same work claims that the flow rate has no significant effect on the crystal size. In contrast, our in situ observation reveals that higher flow rates result in smaller crystals. Guided by our prediction, we intentionally increased MoO_3 growth temperature and decreased flow rate in several additional growth trials. A significant increase in crystal size is obtained at a combined condition of a high MoO_3 temperature of 876 °C and low flow rate of 70 sccm (Figure 3b) compared to the baseline condition (~800 °C and ~200 sccm). Decreasing the temperature to ~800 °C but retaining the low flow rate of 70 sccm reduces the crystal size (Figure 3c), which is nonetheless still larger than the baseline condition. When the flow rate is increased to 290 sccm, the crystal size becomes considerably smaller (Figure 3d). In summary, a new experimental condition to produce MoS_2 monolayers with larger crystal size is identified with guidance from machine-learning prediction.

A Nakaya diagram, which is also known as "a letter from the sky", allows one to infer the temperature and humidity of upper atmosphere from the shape of snowflakes without direct measurement.[39] The underlying logic is that humidity and temperature effectively determine the morphology of snowflakes. The same thinking can be applied to CVD growth of MoS_2 crystals. As such, we examined the possibility of extracting the growth conditions from the morphology parameters of MoS_2 monolayers. The term "a letter from the glow" is adopted as we intend to use the growth footage (letter) to decipher growth (glowing at growth temperature) parameters. Similar to the feature analysis in the previous section, the linear regression method is used to analyze the correlation between multiple morphology parameters (X), which serve as input features here, and the growth condition parameters (Y). The correlation among different morphology parameters is first examined (Figure S10) and the nucleation

https://doi.org/10.1021/acs.nanolett.3c04016
Nano Lett. 2024, 24, 2465−2472

density is excluded in the model due to their high correlation (>0.7) to more than one growth parameter in the matrix. A multiple linear regression machine-learning model is then established based on the refined data set (Figure 4a). The model uses the morphology parameters extracted from a film (Figure 4b) as inputs and predicts the growth parameters. In this particular example, predicted growth conditions including MoO_3 temperature, S temperature, and S weight are in good agreement with actual experimental values (Figure 4c). We think this is a simple yet powerful demonstration of the idea of "a letter from the glow", while its accuracy and applicability could be further improved in the future based on a larger amount of experimental data and more detailed characterization of crystal morphologies and their dynamic evolutions.

Growth of the MoS_2 monolayer by CVD was captured in real time using our customized miniaturized CVD apparatus under an optical microscope. The captured footage covered important features of MoS_2 growth, including time-dependent crystal nucleation, growth, and mergence. Morphological parameters including nucleation density and rate, crystal growth rate, final crystal coverage, average crystal size, and edge length can be quantitatively obtained by digitizing growth footage with image processing algorithms. The importance of growth control factors in determining the MoS_2 morphology was determined by using a machine-learning algorithm. The machine-learning model predicted that, at high growth temperature and with low flow rate, MoS_2 crystals with large lateral size can be grown, and experiments successfully validated the prediction—larger than 20 μm single crystalline monolayer MoS_2 triangles were grown at higher than 800 °C temperature and less than 70 sccm carrier gas flow rate. The model also provided close feedback on growth condition parameters based on analysis of the growth footage. Our system and the corresponding workflow established in this work including the growth capturing, digitizing, and machine-learning can work for CVD growth of other 2D materials as well as their heterostructures, therefore offering a powerful platform to understand and control 2D crystal growth and shedding light onto new interdisciplinary areas such as the reverse engineering of materials as well as the data-driven and AI-enabled material design.

■ ASSOCIATED CONTENT

Supporting Information

The Supporting Information is available free of charge at The Supporting Information is available free of charge at https://pubs.acs.org/doi/10.1021/acs.nanolett.3c04016.

Example of unprocessed growth footage (MP4)

Example of processed growth footage (MP4)

Experimental methods; miniature CVD setup (Figure S1); Raman spectra of MoS_2 grown by miniature CVD on sapphire (Figure S2); PL spectra of MoS_2 grown by miniature CVD on sapphire (Figure S3); AFM of MoS_2 grown by miniature CVD on sapphire (Figure S4); PL mapping of MoS_2 flakes grown in the miniature CVD (Figure S5); gallery of original and processed images from MoS_2 growth footage (Figure S6); typical growth footage processed at elapsing time instants (Figure S7); processed growth footage with massive crystal mergence, time-dependent crystal number curve (Figure S8); correlation matrix of the CVD growth parameters (Figure S9); correlation matrix of morphology parameters (Figure S10); parity plots for growth guidance features selected by RFA, RFE, and exhaustive search (Figure S11); growth process features selected and ranking of importance for each morphology parameter (Figure S12); summarized data set (Table S1) (PDF)

■ AUTHOR INFORMATION

Corresponding Authors

Ming Tang − *Department of Materials Science and NanoEngineering, Rice University, Houston, Texas 77005, United States;* orcid.org/0000-0001-7194-3485; Email: mt20@rice.edu

Jun Lou − *Department of Materials Science and NanoEngineering, Rice University, Houston, Texas 77005, United States; Department of Chemistry, Rice University, Houston, Texas 77005, United States;* orcid.org/0000-0002-4351-9561; Email: jlou@rice.edu

Authors

Jing Zhang − *Department of Materials Science and NanoEngineering, Rice University, Houston, Texas 77005, United States;* orcid.org/0000-0002-4706-8630

Tianshu Zhai − *Department of Materials Science and NanoEngineering, Rice University, Houston, Texas 77005, United States*

Faizal Arifurrahman − *Department of Materials Science and NanoEngineering, Rice University, Houston, Texas 77005, United States*

Yuguo Wang − *Department of Materials Science and NanoEngineering, Rice University, Houston, Texas 77005, United States*

Andrew Hitt − *Department of Materials Science and NanoEngineering, Rice University, Houston, Texas 77005, United States*

Zelai He − *Department of Materials Science and NanoEngineering, Rice University, Houston, Texas 77005, United States*

Qing Ai − *Department of Materials Science and NanoEngineering, Rice University, Houston, Texas 77005, United States;* orcid.org/0000-0002-6086-5431

Yifeng Liu − *Department of Materials Science and NanoEngineering, Rice University, Houston, Texas 77005, United States*

Chen-Yang Lin − *Department of Materials Science and NanoEngineering, Rice University, Houston, Texas 77005, United States*

Yifan Zhu − *Department of Materials Science and NanoEngineering, Rice University, Houston, Texas 77005, United States;* orcid.org/0000-0002-9816-5764

Complete contact information is available at: https://pubs.acs.org/10.1021/acs.nanolett.3c04016

Author Contributions

[§]J.Z. and T.Z. contributed equally to this work.

Notes

The authors declare no competing financial interest.

■ ACKNOWLEDGMENTS

J.Z., T.Z., Y.Z., and J.L acknowledge support from the Welch foundation grant (C-1716) and the NSF I/UCRC Center for Atomically Thin Multifunctional Coatings (ATOMIC) under award # EEC-2113882. F.A. is supported by the Fulbright

Scholar Program and the National Science Foundation under project CMMI-1929949. A.H. acknowledges support from Air Force Office of Scientific Research through Grant No. FA9550-21-1-0460. M.T. is supported by the Department of Energy, Basic Energy Sciences under project DE-SC0019111.

REFERENCES

(1) Zhang, Y.; Zhang, L.; Zhou, C. Review of Chemical Vapor Deposition of Graphene and Related Applications. *Acc. Chem. Res.* **2013**, *46* (10), 2329−2339.
(2) Zhang, K.; Feng, Y.; Wang, F.; Yang, Z.; Wang, J. Two Dimensional Hexagonal Boron Nitride (2D-HBN): Synthesis, Properties and Applications. *J. Mater. Chem. C* **2017**, *5* (46), 11992−12022.
(3) Liu, H. F.; Wong, S. L.; Chi, D. Z. CVD Growth of MoS2-Based Two-Dimensional Materials. *Chemical Vapor Deposition*. Wiley-VCH Verlag, December 1, 2015; pp 241−259. DOI: 10.1002/cvde.201500060.
(4) Zhang, Y.; Yao, Y.; Sendeku, M. G.; Yin, L.; Zhan, X.; Wang, F.; Wang, Z.; He, J. Recent Progress in CVD Growth of 2D Transition Metal Dichalcogenides and Related Heterostructures. *Adv. Mater.* **2019**, *31* (41), 1901694.
(5) Ye, G.; Gong, Y.; Lei, S.; He, Y.; Li, B.; Zhang, X.; Jin, Z.; Dong, L.; Lou, J.; Vajtai, R.; Zhou, W.; Ajayan, P. M. Synthesis of Large-Scale Atomic-Layer SnS2 through Chemical Vapor Deposition. *Nano Res.* **2017**, *10* (7), 2386−2394.
(6) Zhou, X.; Cheng, J.; Zhou, Y.; Cao, T.; Hong, H.; Liao, Z.; Wu, S.; Peng, H.; Liu, K.; Yu, D. Strong Second-Harmonic Generation in Atomic Layered GaSe. *J. Am. Chem. Soc.* **2015**, *137* (25), 7994−7997.
(7) Liang, J.; Fang, Q.; Wang, H.; Xu, R.; Jia, S.; Guan, Y.; Ai, Q.; Gao, G.; Guo, H.; Shen, K.; Wen, X.; Terlier, T.; Wiederrecht, G. P.; Qian, X.; Zhu, H.; Lou, J. Perovskite-Derivative Valleytronics. *Adv. Mater.* **2020**, *32* (48), 2004111.
(8) Wang, S.; Rong, Y.; Fan, Y.; Pacios, M.; Bhaskaran, H.; He, K.; Warner, J. H. Shape Evolution of Monolayer MoS2 Crystals Grown by Chemical Vapor Deposition. *Chem. Mater.* **2014**, *26* (22), 6371−6379.
(9) Yang, S. Y.; Shim, G. W.; Seo, S.-B.; Choi, S.-Y. Effective Shape-Controlled Growth of Monolayer MoS2 Flakes by Powder-Based Chemical Vapor Deposition. *Nano Res.* **2017**, *10* (1), 255−262.
(10) Sharma, R.; Sahoo, K. R.; Rastogi, P. K.; Biroju, R. K.; Theis, W.; Narayanan, T. N. On the Synthesis of Morphology-Controlled Transition Metal Dichalcogenides via Chemical Vapor Deposition for Electrochemical Hydrogen Generation. *Physica Status Solidi - Rapid Research Letters* **2019**, *13* (12), 1900257.
(11) Zhang, Y.; Ji, Q.; Han, G. F.; Ju, J.; Shi, J.; Ma, D.; Sun, J.; Zhang, Y.; Li, M.; Lang, X. Y.; Zhang, Y.; Liu, Z. Dendritic, Transferable, Strictly Monolayer MoS2 Flakes Synthesized on SrTiO3 Single Crystals for Efficient Electrocatalytic Applications. *ACS Nano* **2014**, *8* (8), 8617−8624.
(12) Xu, W.; Li, S.; Zhou, S.; Lee, J. K.; Wang, S.; Sarwat, S. G.; Wang, X.; Bhaskaran, H.; Pasta, M.; Warner, J. H. Large Dendritic Monolayer MoS2 Grown by Atmospheric Pressure Chemical Vapor Deposition for Electrocatalysis. *ACS Appl. Mater. Interfaces* **2018**, *10* (5), 4630−4639.
(13) Zhang, Y.; Zhang, Y.; Ji, Q.; Ju, J.; Yuan, H.; Shi, J.; Gao, T.; Ma, D.; Liu, M.; Chen, Y.; Song, X.; Hwang, H. Y.; Cui, Y.; Liu, Z. Controlled Growth of High-Quality Monolayer WS2 Layers on Sapphire and Imaging Its Grain Boundary. *ACS Nano* **2013**, *7* (10), 8963−8971.
(14) Garcia-Segura, S.; Lanzarini-Lopes, M.; Hristovski, K.; Westerhoff, P. Electrocatalytic Reduction of Nitrate: Fundamentals to Full-Scale Water Treatment Applications. *Applied Catalysis B: Environmental*; Elsevier B.V., November 15, 2018; pp 546−568. DOI: 10.1016/j.apcatb.2018.05.041.
(15) Shinde, S. M.; Dhakal, K. P.; Chen, X.; Yun, W. S.; Lee, J.; Kim, H.; Ahn, J. H. Stacking-Controllable Interlayer Coupling and Symmetric Configuration of Multilayered Mos2. *NPG Asia Mater.* **2018**, *10* (2), e468.
(16) Zhang, J.; Wang, F.; Shenoy, V. B.; Tang, M.; Lou, J. Towards Controlled Synthesis of 2D Crystals by Chemical Vapor Deposition (CVD). *Mater. Today* **2020**, *40*, 132−139.
(17) Wu, Y.; Yang, P. Direct Observation of Vapor-Liquid-Solid Nanowire Growth. *J. Am. Chem. Soc.* **2001**, *123*, 3165−3166.
(18) Yoshida, H.; Takeda, S.; Uchiyama, T.; Kohno, H.; Homma, Y. Atomic-Scale in-Situ Observation of Carbon Nanotube Growth from Solid State Iron Carbide Nanoparticles. *Nano Lett.* **2008**, *8* (7), 2082−2086.
(19) Zhang, K.; Ding, C.; Pan, B.; Wu, Z.; Marga, A.; Zhang, L.; Zeng, H.; Huang, S. Visualizing Van Der Waals Epitaxial Growth of 2D Heterostructures. *Adv. Mater.* **2021**, *33* (45), 2105079.
(20) Jankowski, M.; Saedi, M.; La Porta, F.; Manikas, A. C.; Tsakonas, C.; Cingolani, J. S.; Andersen, M.; De Voogd, M.; Van Baarle, G. J. C.; Reuter, K.; Galiotis, C.; Renaud, G.; Konovalov, O. V.; Groot, I. M. N. Real-Time Multiscale Monitoring and Tailoring of Graphene Growth on Liquid Copper. *ACS Nano* **2021**, *15* (6), 9638−9648.
(21) Saedi, M.; De Voogd, J. M.; Sjardin, A.; Manikas, A.; Galiotis, C.; Jankowski, M.; Renaud, G.; La Porta, F.; Konovalov, O.; Van Baarle, G. J. C.; Groot, I. M. N. Development of a Reactor for the in Situ Monitoring of 2D Materials Growth on Liquid Metal Catalysts, Using Synchrotron x-Ray Scattering, Raman Spectroscopy, and Optical Microscopy. *Rev. Sci. Instrum.* **2020**, *91* (1), 013907.
(22) Zhou, D.; Shu, H.; Hu, C.; Jiang, L.; Liang, P.; Chen, X. Unveiling the Growth Mechanism of MoS2 with Chemical Vapor Deposition: From Two-Dimensional Planar Nucleation to Self-Seeding Nucleation. *Cryst. Growth Des* **2018**, *18* (2), 1012−1019.
(23) Zhu, D.; Shu, H.; Jiang, F.; Lv, D.; Asokan, V.; Omar, O.; Yuan, J.; Zhang, Z.; Jin, C. Capture the Growth Kinetics of CVD Growth of Two-Dimensional MoS2. *NPJ. 2D Mater. Appl.* **2017**, *1* (8), 1−7.
(24) Rasouli, H. R.; Mehmood, N.; Çakıroğlu, O.; Kasırga, T. S. Real time optical observation and control of atomically thin transition metal dichalcogenide synthesis. *Nanoscale* **2019**, *11* (15), 7317−7323.
(25) Xue, H.; Wu, G.; Zhao, B.; Wang, D.; Wu, X.; Hu, Z. High-temperature in situ investigation of chemical vapor deposition to reveal growth mechanisms of monolayer molybdenum disulfide. *ACS Applied Electronic Materials* **2020**, *2* (7), 1925−1933.
(26) Taheri, P.; Wang, J.; Xing, H.; Destino, J. F.; Arik, M. M.; Zhao, C.; Kang, K.; Blizzard, B.; Zhang, L.; Zhao, P.; Huang, S.; Yang, S.; Bright, F. V.; Cerne, J.; Zeng, H. Growth Mechanism of Largescale MoS2Monolayer by Sulfurization of MoO3 Film. *Mater. Res. Express* **2016**, *3* (7), 075009.
(27) Yang, L.; Wang, D.; Liu, M.; Liu, H.; Tan, J.; Wang, Z.; Zhou, H.; Yu, Q.; Wang, J.; Lin, J.; Zou, X.; Qiu, L.; Cheng, H.-M.; Liu, B. Glue-Assisted Grinding Exfoliation of Large-Size 2D Materials for Insulating Thermal Conduction and Large-Current-Density Hydrogen Evolution. *Mater. Today* **2021**, *51*, 145−154.
(28) Dumcenco, D.; Ovchinnikov, D.; Marinov, K.; Lazić, P.; Gibertini, M.; Marzari, N.; Lopez Sanchez, O.; Kung, Y.-C.; Krasnozhon, D.; Chen, M.-W.; Bertolazzi, S.; Gillet, P.; Fontcuberta i Morral, A.; Radenovic, A.; Kis, A. Large-Area Epitaxial Monolayer MoS2. *ACS Nano* **2015**, *9* (4), 4611−4620.
(29) Van Der Zande, A. M.; Huang, P. Y.; Chenet, D. A.; Berkelbach, T. C.; You, Y.; Lee, G. H.; Heinz, T. F.; Reichman, D. R.; Muller, D. A.; Hone, J. C. Grains and Grain Boundaries in Highly Crystalline Monolayer Molybdenum Disulphide. *Nat. Mater.* **2013**, *12* (6), 554−561.
(30) Costine, A.; Delsa, P.; Li, T.; Reinke, P.; Balachandran, P. V. Data-Driven Assessment of Chemical Vapor Deposition Grown MoS2Monolayer Thin Films. *J. Appl. Phys.* **2020**, *128*, 235303.
(31) Mao, Y.; Dong, N.; Wang, L.; Chen, X.; Wang, H.; Wang, Z.; Kislyakov, I. M.; Wang, J. Machine Learning Analysis of Raman Spectra of MoS2. *Nanomaterials* **2020**, *10* (11), 2223.
(32) Tang, B.; Lu, Y.; Zhou, J.; Chouhan, T.; Wang, H.; Golani, P.; Xu, M.; Xu, Q.; Guan, C.; Liu, Z. Machine Learning-Guided Synthesis of Advanced Inorganic Materials. *Mater. Today* **2020**, *41*, 72−80.

https://doi.org/10.1021/acs.nanolett.3c04016
Nano Lett. 2024, 24, 2465−2472

(33) Patra, T. K.; Zhang, F.; Schulman, D. S.; Chan, H.; Cherukara, M. J.; Terrones, M.; Das, S.; Narayanan, B.; Sankaranarayanan, S. K. R. S. Defect Dynamics in 2-D MoS2 Probed by Using Machine Learning, Atomistic Simulations, and High-Resolution Microscopy. *ACS Nano* **2018**, *12* (8), 8006−8016.
(34) Najmaei, S.; Liu, Z.; Zhou, W.; Zou, X.; Shi, G.; Lei, S.; Yakobson, B. I.; Idrobo, J. C.; Ajayan, P. M.; Lou, J. Vapour Phase Growth and Grain Boundary Structure of Molybdenum Disulphide Atomic Layers. *Nat. Mater.* **2013**, *12* (8), 754−759.
(35) Lee, C.; Yan, H.; Brus, L. E.; Heinz, T. F.; Hone, J.; Ryu, S. Anomalous Lattice Vibrations of Single- and Few-Layer MoS2. *ACS Nano* **2010**, *4* (5), 2695−2700.
(36) Amani, M.; Lien, D.-H.; Kiriya, D.; Xiao, J.; Azcatl, A.; Noh, J.; Madhvapathy, S. R.; Addou, R.; KC, S.; Dubey, M.; Cho, K.; Wallace, R. M.; Lee, S.-C.; He, J.-H.; Ager, J. W.; Zhang, X.; Yablonovitch, E.; Javey, A. Near-Unity Photoluminescence Quantum Yield in MoS2. *Science (1979)* **2015**, *350* (6264), 1065−1068.
(37) Lanzillo, N. A.; Glen Birdwell, A.; Amani, M.; Crowne, F. J.; Shah, P. B.; Najmaei, S.; Liu, Z.; Ajayan, P. M.; Lou, J.; Dubey, M.; Nayak, S. K.; O'Regan, T. P. Temperature-Dependent Phonon Shifts in Monolayer MoS2. *Appl. Phys. Lett.* **2013**, *103* (9), 093102.
(38) Liu, H. Feature Selection. In *Encyclopedia of Machine Learning*; Sammut, C., Webb, G. I., Eds.; Springer US: Boston, MA, 2010; pp 402−406. DOI: 10.1007/978-0-387-30164-8_306.
(39) Libbrecht, K. G. Toward a Comprehensive Model of Snow Crystal Growth Dynamics: 1. Overarching Features and Physical Origins. *arXiv:1211.5555* **2012**, DOI: 10.48550/arXiv.1211.5555.

https://doi.org/10.1021/acs.nanolett.3c04016
Nano Lett. 2024, 24, 2465−2472